TOPICAL REVIEW

# On-surface synthesis on a bulk insulator surface



IOP Publishing Journal of Physics: Condensed Matter
J. Phys.: Condens. Matter **30** (2018) 133001 (15pp) https://doi.org/10.1088/1361-648X/aab0b9

## Topical Review

# On-surface synthesis on a bulk insulator surface

**Antje Richter[1], Andrea Floris[2], Ralf Bechstein[1], Lev Kantorovich[3] and Angelika Kühnle[1,4]**

[1] Institute of Physical Chemistry, Johannes Gutenberg University Mainz, Duesbergweg 10-14, 55099 Mainz, Germany
[2] School of Mathematics and Physics, University of Lincoln, Brayford Pool, Lincoln LN6 7TS, United Kingdom
[3] Department of Physics, King's College London, London WC2R 2LS, United Kingdom
[4] Department of Chemistry, Physical Chemistry I, Bielefeld University, Universitätsstraße 25, 33615 Bielefeld, Germany

E-mail: afloris@lincoln.ac.uk and angelika.kuehnle@uni-bielefeld.de

Received 21 December 2017, revised 8 February 2018
Accepted for publication 20 February 2018
Published 8 March 2018

**Abstract**

On-surface synthesis has rapidly emerged as a most promising approach to prepare functional molecular structures directly on a support surface. Compared to solution synthesis, performing chemical reactions on a surface offers several exciting new options: due to the absence of a solvent, reactions can be envisioned that are otherwise not feasible due to the insolubility of the reaction product. Perhaps even more important, the confinement to a two-dimensional surface might enable reaction pathways that are not accessible otherwise. Consequently, on-surface synthesis has attracted great attention in the last decade, with an impressive number of classical reactions transferred to a surface as well as new reactions demonstrated that have no classical analogue.

So far, the majority of the work has been carried out on conducting surfaces. However, when aiming for electronic decoupling of the resulting structures, e.g. for the use in future molecular electronic devices, non-conducting surfaces are highly desired. Here, we review the current status of on-surface reactions demonstrated on the (10.4) surface of the bulk insulator calcite. Besides thermally induced C–C coupling of halogen-substituted aryls, photochemically induced [2 + 2] cycloaddition has been proven possible on this surface. Moreover, experimental evidence exists for coupling of terminal alkynes as well as diacetylene polymerization. While imaging of the resulting structures with dynamic atomic force microscopy provides a direct means of reaction verification, the detailed reaction pathway often remains unclear. Especially in cases where the presence of metal atoms is known to catalyze the corresponding solution chemistry reaction (e.g. in the case of the Ullmann reaction), disclosing the precise reaction pathway is of importance to understand and generalize on-surface reactivity on a bulk insulator surface. To this end, density-functional theory calculations have proven to provide atomic-scale insights that have greatly contributed to unravelling the details of on-surface synthesis on a bulk insulator surface.

Keywords: on-surface synthesis, bulk insulator, calcite, dynamic atomic force microscopy, molecular electronics, electronic decoupling, density functional theory

(Some figures may appear in colour only in the online journal)

 

## 1. Introduction

On-surface synthesis has emerged as a very promising approach to prepare functional molecular structures directly on a supporting surface [1–3]. In contrast to molecular self-assembly, which relies on the formation of reversible bonds [4], on-surface synthesis aims to create covalent bonds directly on the surface of interest. Thus, long-term stable structures can be created that hold great promise for applications, e.g. for surface functionalization and molecular electronics. On-surface synthesis opens up the possibility to create molecular structures that might not be feasible by classical solution chemistry due to the limited solubility of the products. This is why it is highly interesting in the context of fabricating graphene nanoribbons with tailored electronic structure for future molecular electronics devices [5, 6]. Perhaps even more exciting, the confinement of the molecular precursors upon adsorption onto a surface might enable novel reaction pathways that might not exist in solution. At present, however, many details of on-surface synthesis including potential new reaction pathways await their discovery.

In 2000, Rieder's research group presented a pivotal study carried out in ultrahigh vacuum (UHV) [7], inducing all steps of a classical Ullmann coupling reaction [8] with the tip of a scanning tunneling microscope (STM), creating biphenyl from iodobenzene precursor molecules on a Cu(1 1 1) surface. Another key example using the STM tip to initiate an on-surface reaction has been diacetylene polymerization on graphite, which results in conjugated structures [9, 10], that are highly interesting for creating electrically conductive contacts on a surface. Recently, even triangulene, which has not been isolated before due to its reactivity, has been demonstrated to be synthesized upon tip-induced dehydrogenation of a precursor molecule [11]. However, using the STM tip to initiate a reaction is very time-consuming and, thus, likely to be limited to fundamental studies. In contrast, when using photochemical or thermal initiation, on-surface synthesis can be performed in a parallel manner.

One of the first examples demonstrating the thermal initiation of an on-surface covalent linking was presented by Grill *et al* in 2007 [12]. In this study, an Ullmann-like reaction has been performed using bromine substituted porphyrin molecules on Au(1 1 1). Depending on the number of substitutions, dimers, linear chains or extended networks have been obtained. Later, the same group extended their strategy by inducing a hierarchical approach, which makes use of the different aryl-halogen bond strength when comparing bromine and iodine substituted porphyrins [13]. This idea allows for a controlled step-by-step linkage of the molecular precursors, which greatly enriches the library of the resulting structures. By now, ten years after Grill's seminal work, a multitude of different reactions have been proven possible on various conducting substrates, including Ullmann-like coupling [12–16], cyclodehydrogenation [17], Glaser-like coupling of terminal alkynes [18–22], condensation reactions—e.g. boronic acid-based chemistry [23–25] and imine [26] as well as polyimide [27] and polyamide [28] network formation—cycloaddition [29] as well as click [30] and deoxygenation reactions [31, 32]. Both the promising potential of on-surface synthesis in future applications and the gain in fundamental understanding alike have stimulated an impressive number of studies in the field of on-surface synthesis.

Still, the vast majority of the above-mentioned studies have been carried out on metal surfaces, with only a few exceptions being highly oriented pyrolytic graphite [14, 22] and semiconductor surfaces [33, 34]. This limitation to metal substrates is mainly due to the fact that STM is frequently used for imaging the resulting structures. Moreover, also many other complementary surface science characterization methods rely on the use of an electrically conductive sample, so metal substrates have been a natural choice from an experimental point of view. In the context of on-surface synthesis, another, perhaps even more important, aspect needs to be considered: many of the above-mentioned reactions that have been transferred from solution chemistry, such as Ullmann or Glaser coupling, are known to be catalyzed by the presence of metal atoms. Thus, also from this fundamental point of view, metal substrates have shown superior performance in on-surface synthesis and it is proven that the choice of the specific substrate has a significant impact on the reaction [14]. However, especially in the context of applications in future molecular electronic devices, electrically non-conducting substrates are interesting as they allow for decoupling of the molecules' electronic structure from the underlying support surface. This is mandatory for avoiding leakage currents, e.g. in molecular wires, when synthesizing a conjugated molecular structure directly on a surface. A very successful solution is to use thin insulator films placed on top of a metal substrate for bond formation [35–39], as in this case STM imaging is still possible, but, at the same time, greatly reduce—or even eliminate—possible leakage currents. However, this approach requires an additional step of preparing the thin film and it has so far been restricted to a rather limited class of insulator materials. In fact, a vast majority of the above-mentioned studies has been conducted on thin films of sodium chloride, with only very few exceptions such as xenon [11]. Thus, it remains highly interesting to extend the existing insights to bulk insulator substrates. With the advent of scanning force microscopy, it has become possible to collect atomically resolved images of bulk insulator surface, providing the option to explore on-surface synthesis on bulk insulators as well.

So far, however, transferring the developed on-surface synthesis strategies to bulk insulator surfaces has posed great experimental challenges. Besides the above-mentioned fundamental limitations in initiating the reaction in the absence of a catalytically active metal, yet another practical limitation has proven to pose substantial hurdle to on-surface synthesis on bulk insulators, which is the weak interaction of the precursor molecules with prototypical insulator surfaces [40, 41] as compared to metal surfaces. Because of this weak interaction, which can be related to the low surface energy of many insulator surfaces, many molecules are prone to desorption at temperatures lower than those needed to initiate an on-surface reaction. This is why substantial effort has been put into designing precursors that, besides possessing a reactive site for on-surface linkage, also feature a functional group that can

act as an anchor towards the surface. In this respect, the bulk insulator calcite has been proven to be an advantageous substrate, for which experimental evidence has been presented demonstrating several on-surface reactions carried out in UHV [2].

As on-surface synthesis in UHV is a rapidly growing research field, this review cannot provide a comprehensive list of studies regarding on-surface synthesis, but will be limited to examples carried out on the natural cleavage plane of calcite. It is intended to give a concise overview of the reactions that have been tested on this surface experimentally and provide a state-of-the-art theoretical insight into a specific system to address the challenging question as to why C–C coupling is possible even in the absence of catalytically active metal atoms.

## 2. Materials and methods

### *2.1. Calcite (10.4) and organic precursors*

In this topical review, the current status of on-surface synthesis on the (10.4) natural cleavage plane of calcite, a bulk insulator with a band gap of about 6 eV [42], is presented. The surface is composed of calcium cations and carbonate anions as shown in the model in figure 1(a). There are two different orientations of the carbonate groups in the surface plane; this is why the surface unit cell consists of two calcium ions and two carbonate groups. Besides the identity, the (10.4) surface possesses only one symmetry operation, which is a glide reflection.

As molecular precursors, small organic molecules have been used. The structural models of all molecules discussed here are given in figure 1(b). The proof-of-principle for on-surface C–C coupling has been presented using halogen substituted benzoic acid derivatives [43], namely 2,5-diiodobenzoic acid (DIBA), 2,5-dichlorobenzoic acid (DCBA), 3,5-diiodosalicylic acid (DISA), and 4-iodobenzoic acid (IBA). The latter molecule has been intensively studied in a theoretical investigation to elucidate the details of the reaction pathway [44]. Moreover, the C–C coupling of precursors possessing two different halogen substitutions has been studied to achieve sequential linking using 2-(4-bromophenyl)-6-(4-chlorophenyl)pyridine-4-carboxylic acid (BPCPPCA) [45]. Next, photochemical initiation has been tested using $C_{60}$ [46]. Diacetylene polymerization has been shown using 3,3′-(1,3-butadiyne-1,4-diyl)-bisbenzoic acid (3BBA) [47] and homocoupling of terminal alkynes with 4,4″-diethynyl-[1,1′:4′,1″-terphenyl]-2′,5′-dicarboxylic acid (DETDCA) molecules as precursors.

### *2.2. Experimental methods: dynamic atomic force microscopy and sample preparation*

For all images shown in this work, dynamic atomic force microscopy (AFM) carried out in UHV using the frequency modulation mode was used, as this technique allows for high-resolution imaging of insulator surfaces. More details about the instrument used in this work can be found in [48]. To this end, a modified variable-temperature scanning force microscope from ScientaOmicron (Taunusstein, Germany) was used. Cantilevers from Nanosensors (Neuchâtel, Switzerland) with eigen-frequencies in the order of 300 kHz and force constants of about 40 N $m^{-1}$ were excited to oscillate with typical oscillation amplitudes of 5–10 nm. The calcite crystals were purchased from Korth Kristalle (Kiel, Germany) and prepared *in vacuo* to arrive at an atomically flat and clean (10.4) surface. Prior to molecule deposition, the surface cleanliness was checked by AFM imaging. All precursor molecules were sublimated *in vacuo* onto a freshly prepared surface. Home-built Knudsen cells were used for this purpose. The required sublimation temperatures were determined in a separate UHV chamber by sublimation onto a quartz crystal microbalance.

### *2.3. Theoretical method: density-functional theory calculations*

Theoretical calculations for the systems presented in this work [44, 47, 49–51] are based on *ab initio* density functional theory (DFT) [52–55]. The analysis of the mechanisms of on-surface synthesis first includes an identification of stable adsorption geometries of molecular units on the substrate (monomers, dimers, chains, 2D networks, etc), i.e. precursors, products and intermediate states. Second, investigations include the calculation of minimum energy paths and activation energy barriers associated with possible reactions on the surface. The most probable mechanism will be the one having the lowest energy barrier, ignoring entropy effects. In the works presented here, these two steps were accomplished, first, by relaxing the DFT forces acting on the whole molecule-substrate system and, second, by performing nudged elastic band [56, 57] calculations. The latter allow characterization of the energy landscape of the surface, the molecular diffusion and the reaction mechanisms. Calculations of geometries and reaction paths were performed at $T = 0$ K [44, 47, 49, 50], while temperature effects were monitored in some cases via *ab initio* molecular dynamics [47, 50]. Several packages were used, including CP2K [58], Quantum-ESPRESSO [59] and VASP [60], within different pseudopotential schemes [61–63] and the GGA-PBE exchange-correlation functional [64]. Dispersion corrections were included at Grimme-D2 [65] and D3 [66] levels.

## 3. Molecule–surface interactions: how to anchor the precursor?

As mentioned above, a critical issue when exploring on-surface synthesis on a bulk insulator surface is the comparatively weak binding of the molecular precursors to many bulk insulator surfaces. This fact can be rationalized by considering the respective surface energies. Compared to metal surfaces having typical surface energies in the range of 1–2 J $m^{-2}$ prototypical insulators such as alkali halides have an order of magnitude smaller surface energies [40]. In this respect, calcite (10.4) is different from other ionic crystal surfaces, as it exhibits a surface energy of 0.59 J $m^{-2}$ when considering the bulk-truncated surface in UHV [67]. From the surface composition of calcite

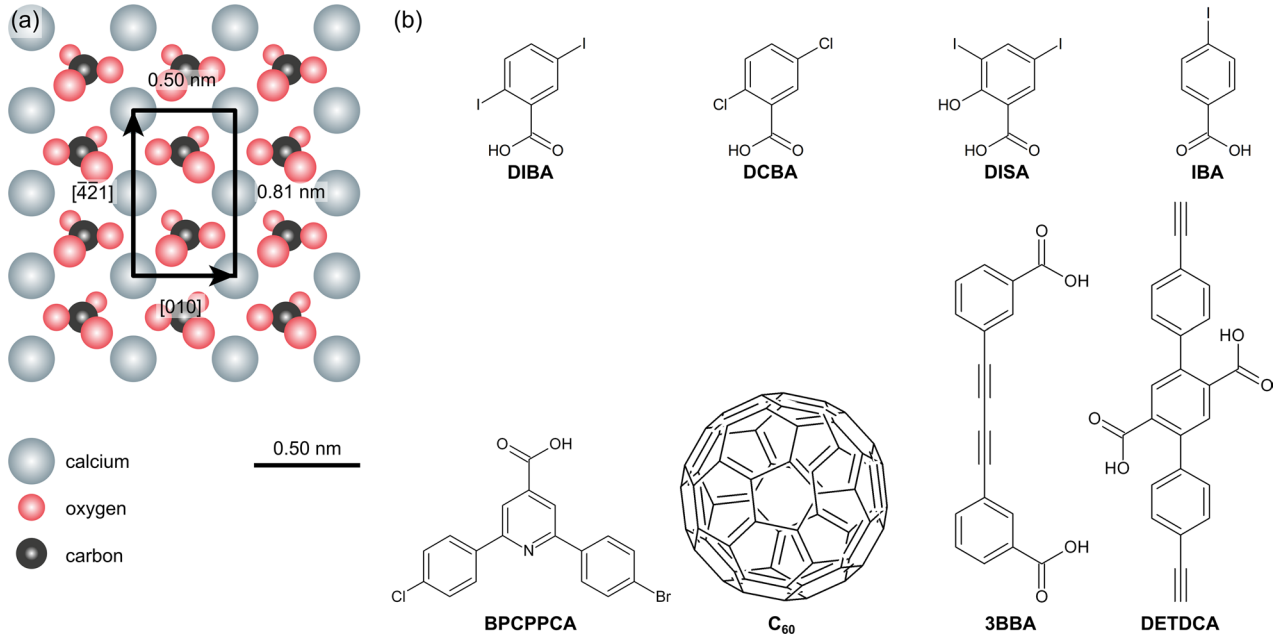


**Figure 1.** (a) Model of the calcite (10.4) cleavage plane. The surface unit cell consists of two calcium ions and two carbonate groups. (b) Compilation of the molecules discussed in this review. The scale bar applies to both subsets.

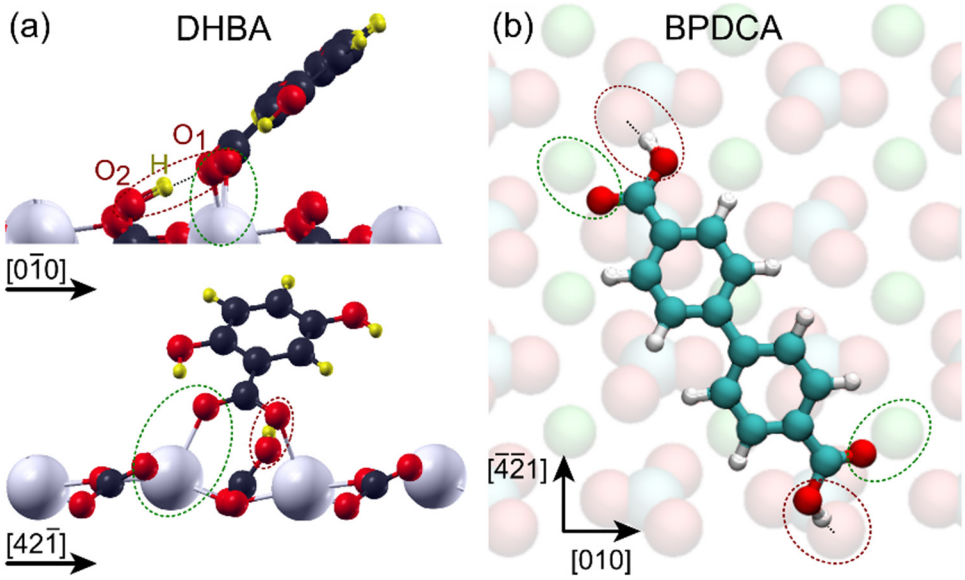


**Figure 2.** Binding configuration of a carboxylic acid group onto calcite (10.4) in (a) an upright position of the 2,5-dihydroxybenzoic acid (DHBA) molecule and (b) lying flat in the case of the biphenyl-4,4′-dicarboxylic acid (BPDCA) molecule. Note that (a) is based on DFT calculations as published in [51], while (b) is a sketch based on the calculations shown in [50]. Reprinted with permission from [50, 51]. Copyright (2016) American Chemical Society.

(10.4), it is evident that electrostatic anchoring to the positively charged calcium ions and the negatively charged carbonate groups is possible. Moreover, from the three oxygen atoms of the carbonate groups, one is below, one in and one protruding the plane defined by the carbon atoms. The protruding oxygen atoms are prone to form bonds, and they are known to offer the option for hydrogen bond formation with hydroxy groups. Therefore, the carboxylic acid group has been identified to offer a suitable anchor functionality, where the negatively charged carbonyl oxygen interacts electrostatically with a surface calcium atom while the hydroxy group forms a hydrogen bond towards the protruding oxygen atom of a neighboring carbonate group [51] (figure 2(a)). DFT calculations [51] have shown that the formation of this hydrogen bond is associated with the hydrogen atom of the carboxylic acid group moving closer toward the protruding oxygen atom of the surface as perhaps expected from the fact that calcite, being the salt of a weak acid, acts as a base. The binding motif of the carboxylic acid group towards calcite favors an upright position of the molecule to optimize the interaction with the surface [68]. However, even when enforcing a flat-lying orientation (figure 2(b)) of the carboxylic acid group by the residual part of the molecule

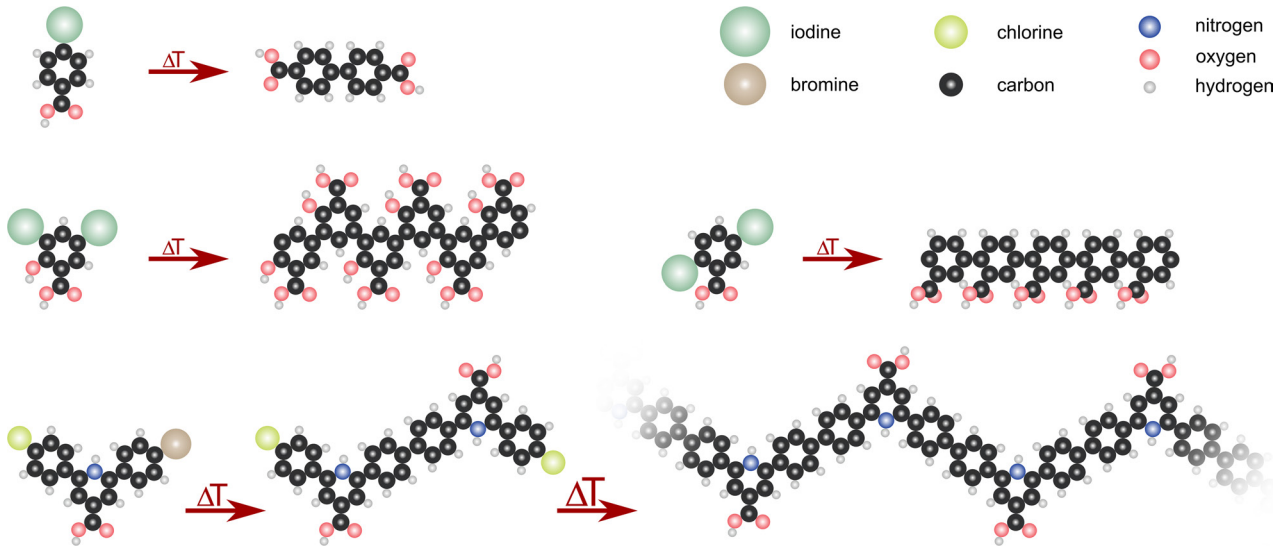


**Figure 3.** Benzoic acid derivatives as a simple building block for on-surface C–C coupling. Depending on the number and position of the halogen atom substitutions, dimers, linear as well as zigzag rows of the molecules can be created. By changing the nature of the substituted atom from iodine to bromine or chlorine, the required reaction temperature can be changed, which opens up a possibility to explore stepwise synthesis reactions.

as in the case of biphenyl-4,4′-dicarboxylic acid (BPDCA), the molecule–surface interaction remains strong enough to observe a templating effect of the calcite substrate [69] due to a preferential binding of the carboxylic acid groups onto the surface [50]. To illustrate the impact of the carboxylic acid group, we can compare desorption experiments of benzene and iodobenzoic acid: while benzene is known to desorb already at about 190 K [70], benzoic acid and iodobenzoic acid are stable on the surface held at room temperature. Furthermore, systematic theoretical calculations of molecules containing different functional groups such as carboxyl, hydroxyl, aldehyde, thiol, amine and nitrile groups interacting with the calcite (10.4) surface, have been performed, yielding information about a wide range of adsorption energies [68, 71]. This allows for a direct comparison of molecules with and without carboxylic acid groups. Exemplarily, acetic acid and benzoic acid yield adsorption energies of 0.98 eV and 1.03 eV, while ethane and benzene result in significantly lower values of 0.17 eV and 0.31 eV, respectively.

Due to the great success with using the carboxylic acid group as an anchor functionality, all molecules discussed here except for $C_{60}$ are equipped with one or two carboxylic acid groups. For $C_{60}$, the size of the molecule and, consequently, its polarizability appear to be large enough to allow for sufficiently strong van der Waals interactions. Besides the carboxylic acid group, also other anchor functionalities can be envisioned such as ester and amide groups or nitrogen in aromatic heterocycles; however, these are not exploited in the studies reviewed here.

## 4. Proof-of-principle: demonstration of aryl–halide coupling on calcite (10.4)

In the classical Ullmann coupling reaction [8], an iodine is cleaved off from a phenyl ring, creating a radical. The cleavage of the bond having a strength of about 270 kJ $mol^{-1}$ is catalyzed by the presence of copper atoms. In the second step, two phenyl radicals combine to form a biphenyl. After impressive demonstrations of the Ullmann coupling on various metal surfaces [12, 14, 16, 72], it has been realized that on-surface synthesis of molecular wires requires electronically decoupling of the molecular electronic structure from the support surface. Therefore, C–C coupling of aryl-halides on the (10.4) surface of the bulk insulator calcite has been explored [43]. To this end, simple benzoic acid derivatives have been studied as they allow for a systematic change of both the number and the position of halogen atom substitutions. Moreover, by changing from iodine to bromine and chlorine, the binding strength can be tuned (figure 3).

### 4.1. Dimerization

When using IBA—having one iodine substitution in *para* position—as a molecular precursor, the on-surface synthesis of the respective dimer, BPDCA, is expected upon C–C coupling. To investigate this, IBA molecules have been deposited onto calcite (10.4) held at room temperature. The precursor molecules are highly mobile on calcite (10.4) and cluster at step edges [73]. As can be seen in figure 4(a), the precursors form an ordered structure that is assumed to be governed by intermolecular hydrogen bond formation. Mild annealing of the substrate to about 500 K is required to arrive at another ordered structure (figure 4(b)), which is characterized by an increased molecule-substrate interaction. In analogy with the binding of a similar molecule to calcite explored in detail by DFT calculations [51], we believe that here, in this wetting layer, the intermolecular hydrogen bonding is broken in favor of a molecule–surface binding, and the molecule's hydrogen atom is expected to be donated to the protruding oxygen atom of the surface. Upon further annealing to 580 K, the structure

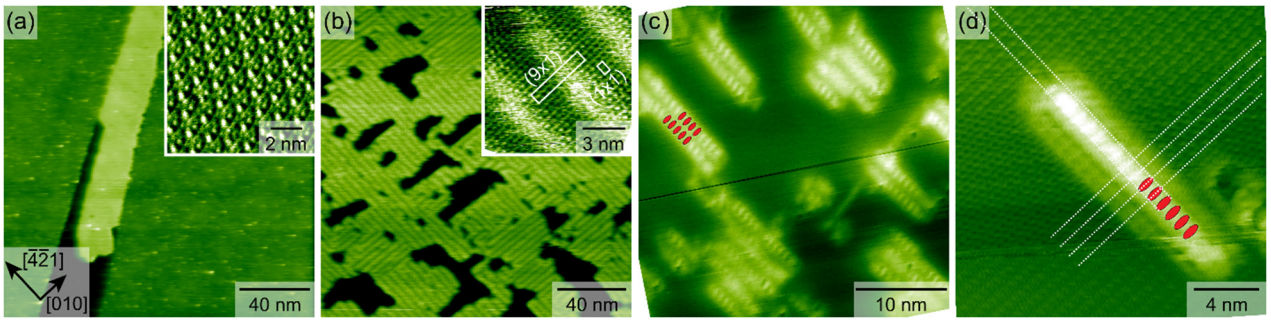


**Figure 4.** (a) Calcite surface after deposition of IBA. Reprinted with permission from [73]. Copyright (2013) American Chemical Society. (b) Upon annealing to about 500 K, the intermolecular hydrogen bonded network breaks and a wetting layer is formed that is governed by hydrogen bonds between the molecules and the substrate. (c) Structure as obtained after annealing to 580 K. (d) High-resolution image showing a molecular row and the atomic structure of the surface simultaneously. BPDCA molecules are superimposed as ellipses to illustrate the envisioned side-by-side alignment of the dimerized IBA molecules. Images (b)–(d) reprinted with permission from [43]. Copyright (2011) American Chemical Society.

again changes substantially. Now, rows composed by side-by-side aligned entities exist on the surface (figure 4(c)). From this image it becomes apparent that the calcite substrate is decisive for the alignment of the rows, which are oriented along the [42$\bar{1}$] substrate direction. In the high-resolution image given in figure 4(d) a single row is shown simultaneously with the atomically resolved calcite surface. In this image, the expected reaction product upon IBA dimerization, namely BPDCA, is superimposed as ellipses onto the molecular features, indicating that the expected reaction indeed took place.

Depending on the local density of molecules, single stripes (figure 4(d)), paired ones or up to five stripes next to each other (figure 4(c)) can be identified. Interestingly, this side-by-side aligned structure can also be found when depositing BPDCA on the surface directly [69], giving further evidence for the fact that the observed rows are composed by the C–C coupled reaction product. However, depositing BPDCA on the surface directly results in a second structure that coexists with the rows formed by side-by-side aligned molecules. In this second structure, the molecules interact in a head-to-tail fashion, indicating that intermolecular hydrogen bonding prevails in this second structure. The absence of the second structure after on-surface synthesis of BPDCA from the precursor IBA can be readily rationalized by the fact that the barrier to break intermolecular hydrogen bonds is overcome already during the first annealing step.

### 4.2. Extended row formation

To give further evidence for the C–C coupling of aryl-halides, the number, position and nature of the halogen substitution has been changed. When increasing the number of iodine atoms at the benzene ring from one to two, extended rows are expected instead of dimers. A confirmation of this approach has been performed using DIBA, having the iodine atoms in 2- and 5-positions, i.e. at the opposite sides of the ring. Consequently, a linear row should be formed upon C–C coupling. Depositing DIBA on the calcite (10.4) surface held at room temperature results in the formation of an ordered wetting layer (figure 5(a)). A substantial structural change can be induced by annealing the substrate above 530 K. Now, rows are formed that are aligned along the [42$\bar{1}$] substrate direction (figure 5(b)). An enlargement of one of these rows given in figure 5(c) reveals an internal structure with a repeat distance of 0.4 nm (figure 5(d)). From this repeat distance, the C–C coupling of the DIBA precursors is deduced, as the distance fits to what would be expected upon covalent linkage.

For a molecule having two reactive sites, the position of these sites can be varied and, thus, the geometry of the resulting structures can be tuned. This has been done with DISA, having the iodine substitutions in 3- and 5-positions. Consequently, a zigzag structure should be possible along with other geometries depending on the specific arrangement of the precursors as illustrated in figure 6(a). When depositing DISA onto calcite (10.4) held at room temperature, a highly ordered wetting layer is obtained (figure 6(b)). Annealing the sample to 580 K induces a significant structural change. Now, irregular-shaped islands exist on the surface as shown in figure 6(c). The rather irregular structure can be understood from the fact that several linking geometries are possible as mentioned above. However, when zooming into the region marked in figure 6(c), a zigzag structure is revealed (figure 6(d)), which fits excellently in its dimensions with the expected structure as illustrated by the superimposed model.

### 4.3. Detailed reaction mechanism: why does it work in the absence of metals?

The phenyl–halide bond strength increases when exchanging iodine by chlorine (phenyl–Cl: 397 kJ mol$^{-1}$ versus phenyl–I: 268 kJ mol$^{-1}$). Thus, when using DCBA instead of DIBA, a similar reaction is expected; however, the structural transition might require higher temperatures. This is indeed the case, as a temperature of 565 K is needed for a DCBA row formation as compared to 530 K for DIBA [43]. However, the simple comparison of the bond strength with the temperature needed to induce radical formation is perhaps misleading, as a classical Ullmann coupling is catalyzed by the presence of copper atoms. The herein reported temperatures required to induce the radial formation are by far too low to allow for cleavage of a bond with a strength in

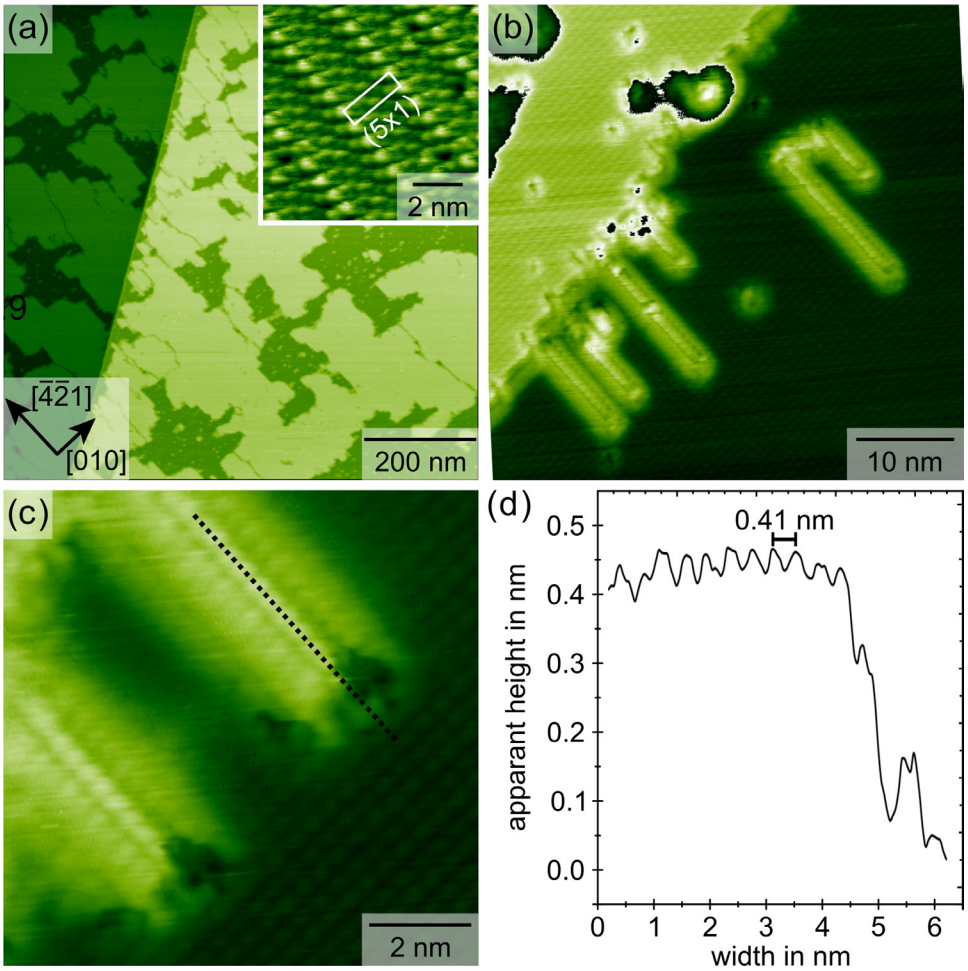


**Figure 5.** (a) Calcite surface after deposition of DIBA. An ordered wetting layer is formed. (b) Upon annealing above 530 K, a substantially different structure is formed, which is characterized by rows running along the [42$\bar{1}$] direction. (c) High-resolution image showing the internal structure of the row. The line profile given in (d) is taken along the direction indicated in (c). Reprinted with permission from [43]. Copyright (2011) American Chemical Society.

the order of 300–400 kJ mol$^{-1}$.[5] Therefore, it is obvious that a specific reaction mechanism has to be at play, which facilitates bond cleavage of these molecules adsorbed on calcite (10.4) even at relatively moderate temperatures. To address this interesting finding and to elucidate the specific reaction mechanism, DFT calculations have been carried out using IBA as a model molecule [44].

As mentioned in section 4.1, the annealing at 580 K of IBA molecules on calcite leads to the formation of chains of dimers oriented along [42$\bar{1}$] (figures 4(c) and (d)). Recent DFT and nudged elastic band calculations [44] have focused on the phenyl–iodine cleavage mechanism, assuming that the corresponding energy barrier dominates the energetics of the whole chains formation process.

The DFT relaxed dimer configuration in figure 7(a) is the final product of the reaction. To reach this configuration, *two* dehalogenations must take place, with an overall energy cost that must be strongly reduced if compared to the one of a single IBA dehalogenation in the gas phase (calculated to be 306 kJ mol$^{-1}$ [44]). By comparing a set of minimum energy paths involving different initial states, two exothermic reaction mechanisms have been found, with strongly reduced energy barriers: the first, realized by a sequence of independent dehalogenations, and the second, where two molecules dehalogenate in a cooperative way.

In the first mechanism (figure 7(b)) a flat molecule undergoes a single dehalogenation on the surface with a barrier of 169 kJ mol$^{-1}$ [44]. This strong barrier reduction is due to the IBA chemisorption upon dehalogenation and the concomitant single iodine adsorption on the substrate. A detailed analysis of the stability of a dehalogenated molecule on the surface reveals in fact that its most stable structure is the one where the flat phenyl radical is chemically bound to a calcite O atom [44]. This chemisorption stabilizes the final state of the reaction and influences the barrier. Clearly, a subsequent molecular diffusion of two dehalogenated IBA molecules is necessary for the dimerization, which is in turn facilitated by the recombinative desorption of $I_2$ molecules. The gas-phase

[5] A rough estimate of the temperature necessary for this reaction to occur can be obtained by assuming a simple Arrhenius law. Taking an attempt frequency of $10^{12}$ s$^{-1}$, the energy barrier of ~3 eV corresponds to a temperature of nearly 1000 K when one-half of the molecules are expected to dissociate after 30 min. This is surely way more than the experimentally required temperature.

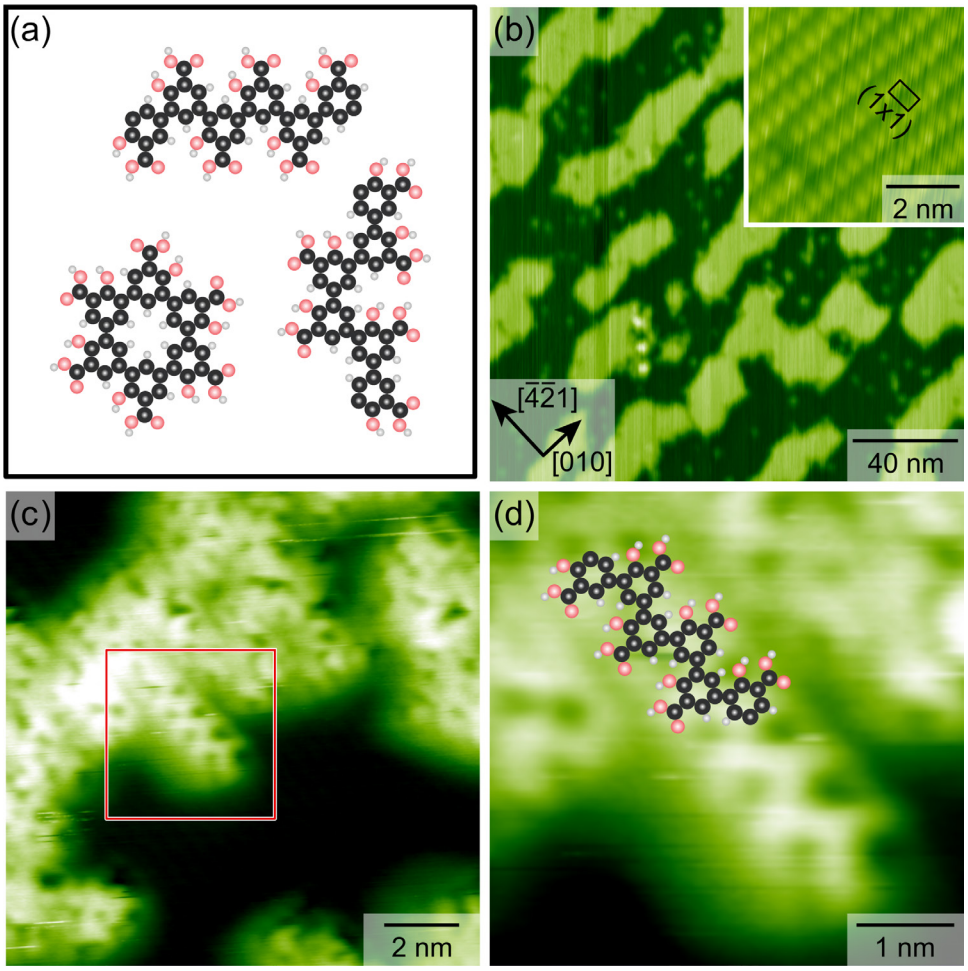


**Figure 6.** (a) Possible structures upon C–C coupling of DISA. (b) Highly ordered wetting layer obtained after depositing DISA onto calcite (10.4) held at room temperature. The inset shows a zoom into the (1 × 1) superstructure. (c) Upon annealing to 580 K, a structural change is revealed. The molecular structure has changed significantly. (d) A zoom into the region marked in (c) reveals a zigzag structure. The superimposed model illustrates the perfect size match with the expected covalently linked structure. Reprinted with permission from [43]. Copyright (2011) American Chemical Society.

recombination of iodines makes the whole process thermodynamically favorable thanks to the large entropic contribution of the $I_2$ gas. Importantly, due to the molecular chemisorption, the insulating substrate clearly plays a catalytic role by reducing the corresponding energy barrier in the total absence of a metallic catalyst.

In the second mechanism (figures 7(c) and (d)), two molecules face each other in an upright configuration. The double dehalogenation is facilitated thanks to the following mechanism [44]: the cost of the first deionization (involving the iodine i1) is reduced, as the second iodine (i2) is first 'exchanged' (figure 7(c), panel 5) and then 'shared' between the two molecules (panel 9). The subsequent i2 detachment is facilitated by the $I_2$ molecule recombination in the gas phase (panel 10), while the dehalogenated IBAs dimerize via the covalent linking between phenyls (panels 10, 13). The overall energy barrier of this nontrivial process is 178 kJ $mol^{-1}$ (figure 7(d)) [44], comparable to the one of the first mechanism. This barrier is far less, however, than the sum of the barriers associated with individual/independent dehalogenations in the gas-phase, as each detachment is somehow 'assisted' by the presence of the other iodine—a certain cooperative mechanism leading to lowering of the barrier. In this second case, however, there is no surface chemisorption. However, the substrate serves as a 2D support to guarantee the molecular confinement, thereby providing the necessary conditions for the reaction to occur. The latter would be hardly met in a 3D environment, again emphasizing the crucial role of the insulating surface.

### *4.4. Towards hierarchical reactions using step-wise C–C coupling*

Exploiting different temperatures to induce the cleavage of the aryl–chlorine and aryl–bromine bond as mentioned above has been proven successful using the precursor molecule BPCPPCA [45]. This molecule is equipped with an iodine and chlorine substitution. When depositing the molecule on the calcite (10.4) surface held at room temperature, molecular islands with a (2 × 4) superstructure are formed on the surface (figure 8(a)). Due to the glide reflection symmetry of the surface, these islands exist in two mirror domains. Within the islands, brighter areas have been observed that have tentatively been ascribed to the second layer [45]. A first structural change could be induced upon annealing the

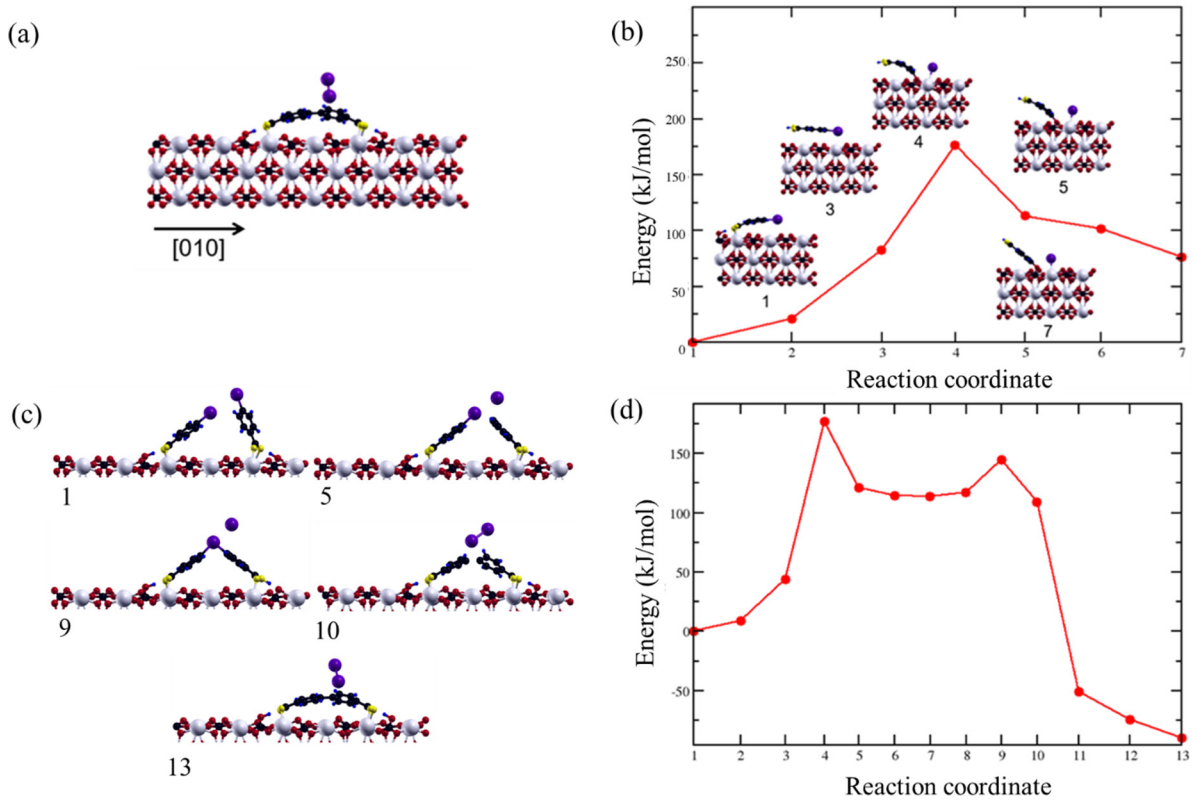


**Figure 7.** (a) IBA dimer configuration, final product after a dehalogenation reaction. (b)–(d) Minimum paths and energy barriers of two main mechanisms of IBA dehalogenation on calcite (10.4) [44]. (a) Independent mechanism: single molecules dehalogenate and chemisorb on the substrate before dimerization. The iodine adsorption is also visible. (c) and (d) Cooperative mechanism of double dehalogenation, as described in the text. In this case, the key factors facilitating the reaction are the two asynchronous dehalogenations, the exchange and sharing of the iodine atoms during the detachments from the molecules, and the $I_2$ recombination. Reaction coordinate numbers correspond to the intermediate molecular configurations shown. Reprinted with permission from [44]. Copyright (2017) American Chemical Society.

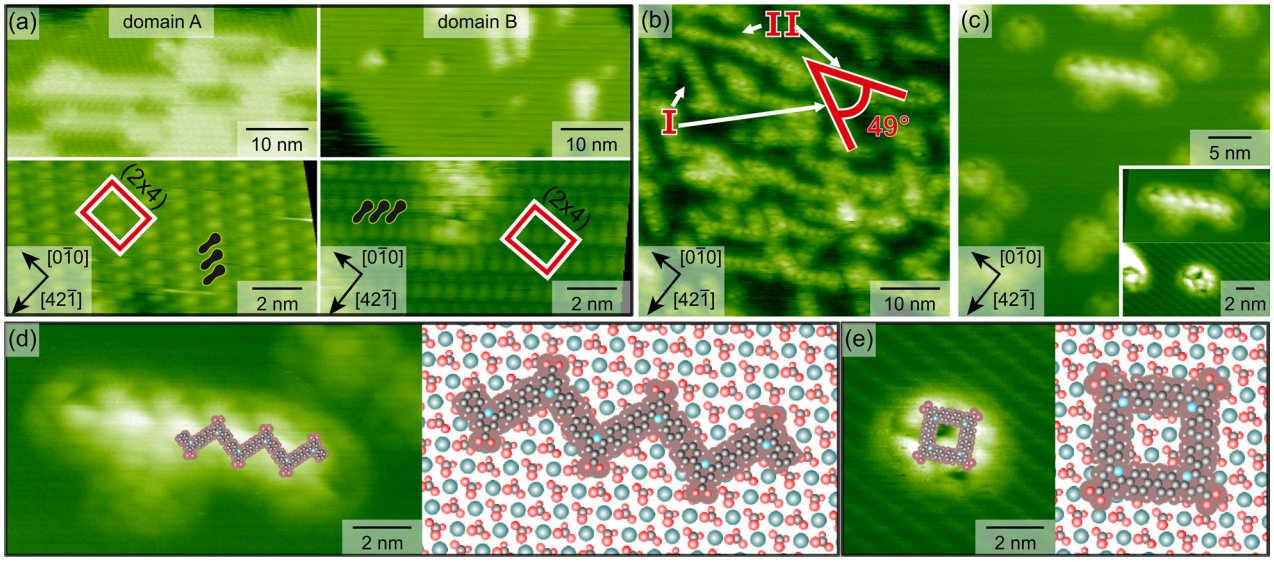


**Figure 8.** (a) As-deposited structure of BPCPPA on a calcite (10.4) surface held at room temperature. Two mirror domains of (2 × 4) islands are formed. (b) After annealing to 570 K, a first structural change is observed. (c) Upon a second annealing step at 610 K, two other structures are formed, namely a zigzag structure (d) and a closed-ring structure (e). The models are given to illustrate the adsorption sites for the carboxylic acid groups. Reprinted with permission from [45]. Copyright (2013) American Chemical Society.

sample to 570 K. A representative image of the sample after this first annealing step is given in figure 8(b). Instead of ordered islands, row-like structures with a specific orientation with respect to the underlying substrate are found on the surface. From the size and the orientation of these rows it appears plausible that the precursors have underwent a first linking reaction upon homolytic cleavage of the bromine atoms. As the precursor is L-shaped, this reaction should

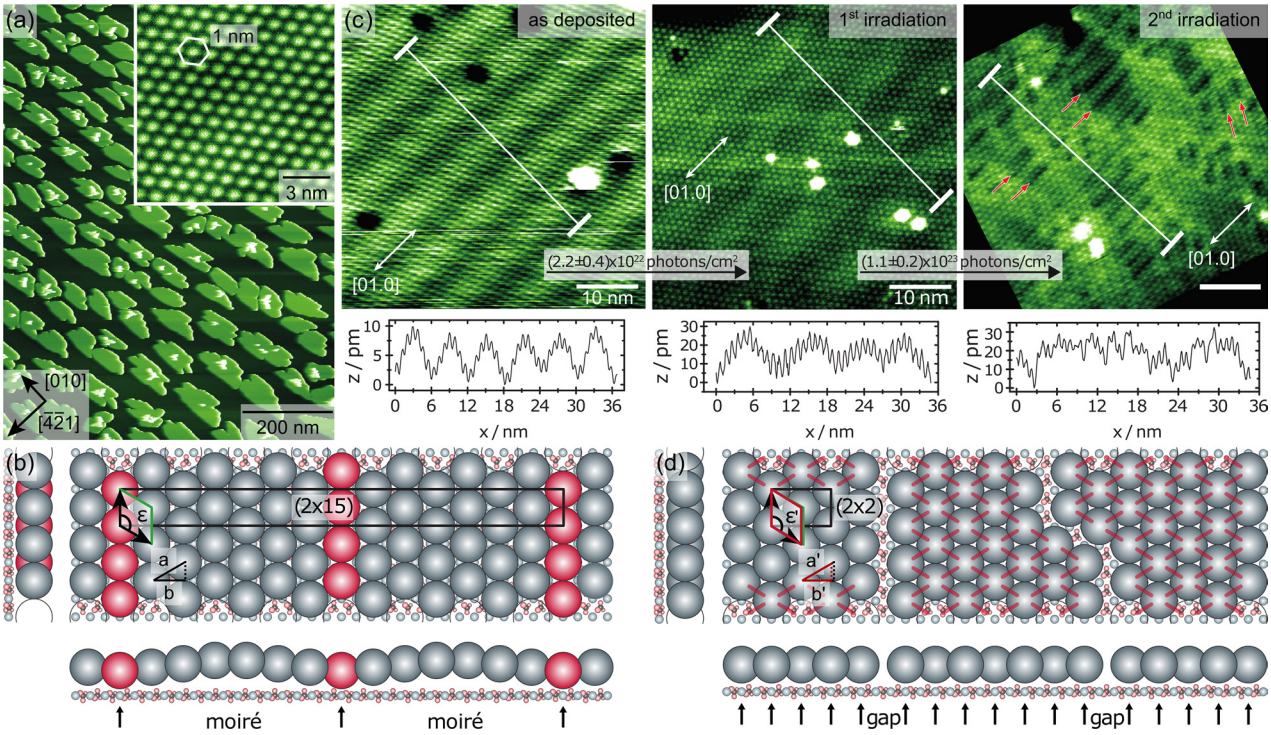


**Figure 9.** (a) Image showing $C_{60}$ islands on calcite (10.4). Reproduced from [41] with permission of The Royal Society of Chemistry. (b) Proposed model explaining the superstructure and the origin for the observed moiré pattern. (c) Image series showing the changes induced upon irradiation of the film with a 405 nm laser diode. (d) Model explaining the preferential reaction direction by a reduction in the lattice mismatch. Images (b)–(d) adapted with permission from [46] John Wiley & Sons. © 2014 WILEY-VCH Verlag GmbH & Co. KGaA, Weinheim.

result in the formation of S- or U-shaped dimers. The row structure formed after annealing suggests that predominantly S-shaped dimers assemble in rows. As envisioned from the molecular design, a second structural transition can be induced when annealing to 610 K. After this annealing step, two different structures have been obtained on the surface as given in figure 8(c). These two structures perfectly match in size and orientation with what would be expected when further linking the S-shaped and the U-shaped dimers. When linking the S-shaped molecules, a zigzag structure should be formed, which is given in the superposition in figure 8(d). For this zigzag structure, the orientation with respect to the surface is not random, as the carboxylic acid anchor requires specific surface sites. The experimentally observed orientation is special in the sense that this orientation ensures the same adsorption position for all carboxylic acid moieties in the zigzag structure. For the closed-ring structure (figure 8(e)), it is not possible to arrive at an orientation, which accommodates the same adsorption site for all four carboxylic acid groups. This might explain why the rings have been imaged with a somewhat asymmetric structure. The precise match of the obtained structures with what has been encoded in the precursor structure provides convincing experimental evidence for the fact that the two-step linkage has been successful. As such, this example demonstrates that also on calcite, a two-step reaction is possible, opening up an exciting option for sequential linkage with site- specificity, which is important for a further hierarchical design of complex molecular structures.

## 5. Exploring further on-surface reactions

The demonstration of aryl–halide coupling presented in the previous section constitutes a first proof-of-principle for on-surface synthesis on the bulk insulator calcite. However, for on-surface synthesis it is desirable to extent the toolbox of possible linking reaction. Moreover, using annealing to initiate the reaction can be difficult for molecules that anchor only weakly onto the surface. Furthermore, as many molecules are deposited by sublimation from a crucible, molecules that are prone to react upon annealing might undergo a linking reaction already in the crucible. Therefore, it is interesting to explore on-surface reactions, stimulated in a different way. Here we shall consider reactions that can be initiated photochemically.

### *5.1. Photochemical [2 + 2] cycloaddition of $C_{60}$ on calcite (10.4)*

The first demonstration of a photochemically initiated reaction on a calcite (10.4) surface has been a [2 + 2] cycloaddition of $C_{60}$ [46]. This reaction is known from bulk $C_{60}$ [74] and has been shown on metal and semiconductor surfaces [75–77]. When deposited onto calcite (10.4), $C_{60}$ forms ordered islands with a [2 × 15] superstructure [41], as shown in figures 9(a) and (b). The lattice mismatch between the $C_{60}$ islands and the calcite lattice gives rise to a moiré pattern, which is manifested by stripes running along the [0 1 0] direction. As a moiré pattern is very sensitive to slight changes in the lattice spacings, it serves as an indicator for changes in the $C_{60}$–$C_{60}$ distance.

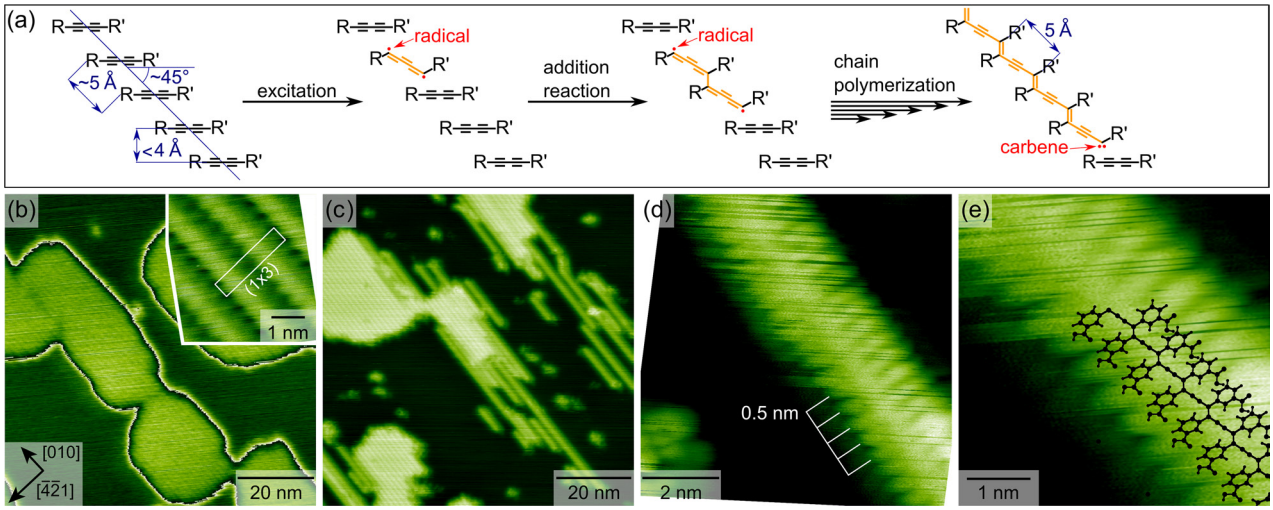


**Figure 10.** (a) Diacetylene reaction scheme inspired by [78]. Reproduced with permission of The Royal Society of Chemistry. (b) Image showing the as-deposited structure of 3BBA on calcite (10.4). (c) Image showing the structural changes upon annealing the sample to 485 K. (d) Close-up of a molecular row. (e) Row structure with superimposed DFT model. Images (b)–(e) reproduced from [47] with permission of The Royal Society of Chemistry.

Upon irradiation with a 405 nm laser diode, the moiré pattern becomes aperiodic and eventually vanishes as shown in the image series in figure 9(c). Interestingly, dark rows appear in the layer (indicated by red arrows in the last image in figure 9(c)), which are predominantly aligned along the [0 1 0] direction. These rows have been explained by the gaps that originate when two $C_{60}$ molecules move closer to form a bond. As most gaps are aligned along the [0 1 0] direction, the majority of the $C_{60}$–$C_{60}$ bonds formed are not oriented along [0 1 0], but form an angle of 60° to this direction. This preferential direction of the bond formation can be understood from the lattice mismatch with the underlying substrate. As illustrated in figure 9(d), the lattice mismatch in [4 2 − 1] direction can be reduced when forming a $C_{60}$–$C_{60}$ bond along the direction marked with an *a*. Before reaction, this distance is about 1 nm, which means that the distance *b* is 0.93 nm. When forming a $C_{60}$–$C_{60}$ bond, the distance *a* is reduced to *a*′, which is about 0.9 nm. This distance reduction implies that the distance *b*′ is now 0.8 nm, which results in a perfect match with the unit cell dimension along the [4 2 $\bar{1}$] direction. Therefore, this work has demonstrated that the choice of the underlying lattice in on-surface synthesis can be used to control the direction in which the reaction proceeds.

### 5.2. Diacetylene polymerization

For contacting functional molecular structures on surfaces, diacetylene polymerization (see scheme in figure 10(a)) has been suggested as a suitable way to produce conjugated molecular wire-like structures on surfaces [78, 79]. Therefore, inducing a diacetylene polymerization on a bulk insulator surface has been explored using 3BBA as precursor molecules [47]. Deposited onto calcite (10.4) held at room temperature, 3BBA forms islands with a (1 × 3) inner structure that is composed of rows running in the [0 1 0] direction as given in figure 10(b). DFT calculations have provided insights into the arrangement of the molecules within these islands, which is governed by a $\pi$–$\pi$ interaction of the aromatic rings. Interestingly, in this arrangement, the molecules adopt a relative orientation and spacing that is required for the diacetylene polymerization [80]. Upon annealing or irradiation, the island structures have been shown to change considerably (figure 10(c)). Now, single molecular rows are found on the surface, which are imaged with a smaller apparent height as compared to the above-mentioned islands. When zooming in, a highly periodic inner structure of the rows can be resolved as shown in figure 10(d). This row structure fits in size with what is expected when forming a diacetylene polymerized strand, as can be seen from the overlay shown in figure 10(e), which is based on DFT calculations. The DFT calculations have revealed the polymerized strands are reduced in height by 0.1 nm as compared to the unreacted assembly, which nicely agrees with the fact that the newly formed single rows have been imaged with a smaller apparent height than the initial 3BBA islands. Thus, the experimental images together with the DFT calculations have provided strong evidence for a successful initiation of a diacetylene polymerization on calcite (10.4).

### 5.3. Coupling of terminal alkynes

Terminal alkynes are known to undergo a homocoupling reaction, which is related to Glaser coupling in solution synthesis [81]. On various metal surfaces, this reaction has been proven possible as a promising route to construct rigid linear linkers [18–21, 82, 83]. For homocoupling of terminal alkynes on calcite (10.4), DETDCA has been chosen as a precursor [84]. This molecule is equipped with two ethynyl groups, which are intended for the on-surface homocoupling. Additionally, it features two carboxylic acid anchors to prevent desorption before reaction. Two different deposition routes have been tested, referred to as low-temperature and high-temperature deposition. For the low-temperature deposition method, the crucible with the molecules has been heated to about 355 K,

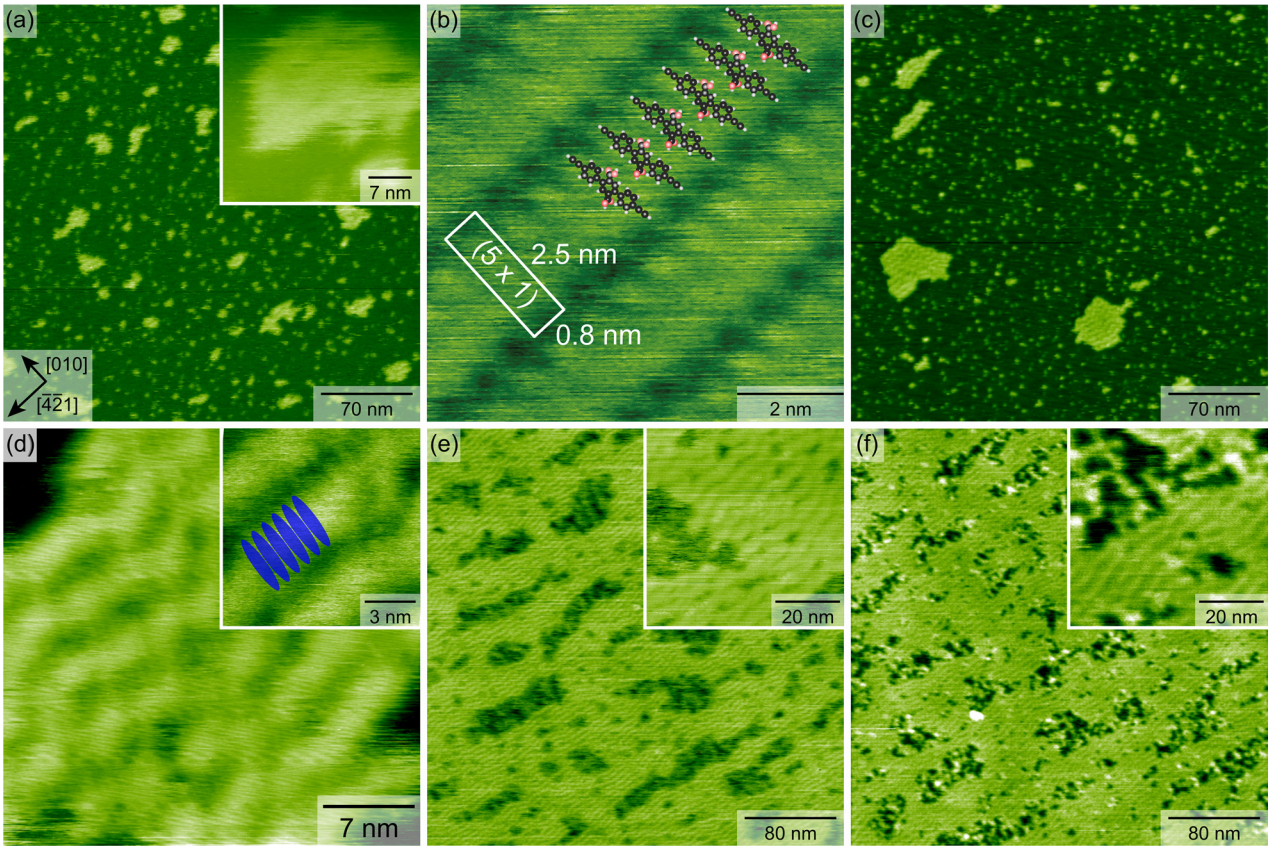


**Figure 11.** (a) Image taken after low-temperature deposition of DETDCA with small surface coverage. (b) When increasing the coverage, an inner structure has been resolved that fits the dimension of the precursor as illustrated by the superimposed model in the inset. (c) Image obtained upon annealing a sample after low-temperature deposition of DETDCA. (d) Zoom into the stripe structure with superimposed ellipses that illustrate the dimerized DETDCA molecules. (e) Islands as obtained after high-temperature deposition of DETDCA. The inset shows a zoom into this structure. (f) Structures obtained after irradiating the high-temperature deposited islands. Reprinted from [84], Copyright 2017, with permission from Elsevier.

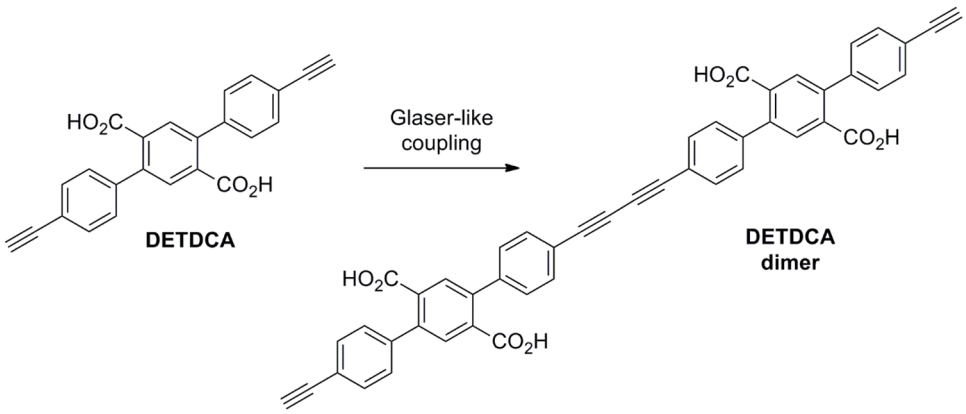


**Scheme 1.** Expected on-surface coupling of DETDCA.

while a crucible temperature of about 445 K has been used for the high-temperature deposition method. In both cases, the sample surface has been kept at room temperature. After low-temperature deposition of DETDCA onto calcite (10.4), islands have been found to be scattered over the surface as shown in figure 11(a). No inner structure has been revealed in these islands, which exhibit rather fuzzy edges (see inset), indicating a high mobility of the precursor molecules. This interpretation has been further corroborated by the fact that many lines exist in the image, which is a well-known sign of diffusing species on the surface. Only after a complete monolayer has been reached, an inner structure has been resolved with a (5 × 1) superstructure and dimensions that fit excellently to the size of the DETDCA precursors (figure 11(b)). When annealing the sample after low-temperature deposition of DETDCA to 555 K, a situation as displayed in figure 11(c) has been revealed. Although the overall appearance has been found to be rather similar, two significant changes have been

observed. First, the islands' perimeters are no longer fuzzy and no streaky features ascribed to diffusing species have been observed after annealing. Second, the inner structure of the islands has changed, now featuring stripes with a width that corresponds to the length of dimerized DETDCA molecules as illustrated in figure 11(d). This change in the dimensions of the inner structure suggests a dimerization of the precursors upon annealing. When using the high-temperature deposition protocol instead, islands as shown in figure 11(e) have been obtained. Interestingly, these islands exhibit an inner structure that resembles the structure found previously after annealing the low-temperature deposited molecules, indicating the assembly of dimers. However, a significant difference can be observed when comparing the structures seen in figure 11(e) with the ones in figure 11(d), which manifests in the streaky features in regions without islands as given in the inset. These results have been explained by the fact that the high-temperature deposition protocol results in dimerization already in the crucible [19], which is why predominantly dimers have been deposited. However, few monomers might still be co-sublimated in this case, which give rise to the diffusing species seen in between the islands. Upon irradiating or annealing this structure, the streaky features in between islands have been observed to vanish (figure 11(f)), which is in perfect agreement with the interpretation that annealing or irradiation of the surface results in dimerization of the few remaining monomers. Thus, these experiments have provided compelling experimental evidence for a homocoupling reaction of terminal alkynes on calcite (scheme 1).

## 6. Conclusions and outlook

In this topical review, we have presented the current state-of-the-art in on-surface synthesis on the bulk insulator calcite. Compared to metal substrates, on-surface synthesis on bulk insulators is challenging due to the fact that molecule-surface binding is typically weak. This weak binding needs to be addressed by the specific design of the precursor molecules that often have to be equipped with anchor functionalities to prevent desorption upon reaction initiation by annealing.

By now, it has proven possible to perform aryl-halide coupling with five different precursor molecules on calcite (10.4). For one model molecule—iodobenzoic acid—detailed DFT insights exist that unraveled the detailed reaction pathway. These calculations have elucidated why the analogy of a classical Ullmann reaction can be induced even in the absence of catalyzing metal atoms. The key mechanism for this is closely related to the binding of the precursors towards the surface and their orientation with respect to each other. The latter can result in nontrivial cooperative mechanisms of double dehalogenation, strongly reducing the activation energy barrier. To extend the available toolbox of possible on-surface reactions, other classical synthesis routes have been explored, including light-induced [2 + 2] cycloaddition of $C_{60}$ molecules. The latter reaction has been demonstrated to be governed by the underlying calcite lattice, demonstrating the potential to guide the reaction direction by a suitable choice of the surface lattice. Moreover, diacetylene polymerization, which is known to highly depend on the correct orientation and spacing of the precursors with respect to each other, has been proven possible. Finally, also homocoupling of terminal alkynes, the analogy of a Glaser coupling in solution synthesis, has been presented.

From these examples it becomes evident that the concepts of on-surface synthesis can be extended to bulk insulator surfaces. Nevertheless, attention has to be paid to design suitable precursors that are tailored to meet the special requirements associated with the chosen bulk insulator substrate. Moreover, there is a lack of in-depth theoretical studies that address the special situation of on-surface synthesis in the case of non-conductive substrates.

## Acknowledgments

This work was supported by the DFG through grant KU1980/8-1. Via our membership of the UK's HEC Materials Chemistry Consortium, which is funded by EPSRC (EP/L000202), this work used the ARCHER UK National Supercomputing Service (www.archer.ac.uk).

## ORCID iDs

Angelika Kühnle https://orcid.org/0000-0003-1214-1006

## References

[1] Gourdon A 2008 On-surface covalent coupling in ultrahigh vacuum *Angew. Chem. Int. Ed.* **47** 6950
[2] Lindner R and Kühnle A 2015 On-surface reactions *ChemPhysChem* **16** 1582
[3] Franc G and Gourdon A 2011 Covalent networks through on-surface chemistry in ultra-high vacuum: state-of-the-art and recent developments *Phys. Chem. Chem. Phys.* **13** 14283
[4] Whitesides G M, Mathias J P and Seto C T 1991 Molecular self-assembly and nanochemistry: a chemical strategy for the synthesis of nanostructures *Science* **254** 1312
[5] de Oteyza D G *et al* 2016 Substrate-independent growth of atomically precise chiral graphene nanoribbons *ACS Nano* **10** 9000
[6] Carbonell-Sanromà E *et al* 2017 Doping of graphene nanoribbons via functional group edge modification *ACS Nano* **11** 7355
[7] Hla S-W, Bartels L, Meyer G and Rieder K-H 2000 Inducing all steps of a chemical reaction with the scanning tunneling microscope tip: towards single molecule engineering *Phys. Rev. Lett.* **85** 2777
[8] Ullmann F 1904 Ueber symmetrische Biphenylderivate *Justus Liebigs Ann. Chem.* **332** 38
[9] Okawa Y and Aono M 2001 Linear chain polymerization initiated by a scanning tunneling microscope tip at designated positions *J. Chem. Phys.* **115** 2317
[10] Okawa Y and Aono M 2001 Materials science: nanoscale control of chain polymerization *Nature* **409** 683
[11] Pavlicek N, Mistry A, Majzik Z, Moll N, Meyer G, Fox D J and Gross L 2017 Synthesis and characterization of triangulene *Nat. Nanotechnol.* **12** 308
[12] Grill L, Dyer M, Lafferentz L, Persson M, Peters M V and Hecht S 2007 Nano-architectures by covalent assembly of molecular building blocks *Nat. Nanotechnol.* **2** 687

[13] Lafferentz L, Eberhardt V, Dri C, Africh C, Comelli G, Esch F, Hecht S and Grill L 2012 Controlling on-surface polymerization by hierarchical and substrate-directed growth *Nat. Chem.* **4** 215

[14] Gutzler R, Walch H, Eder G, Kloft S, Heckl W M and Lackinger M 2009 Surface mediated synthesis of 2D covalent organic frameworks: 1,3,5-tris(4-bromophenyl) benzene on graphite(0 0 1), Cu(1 1 1), and Ag(1 1 0) *Chem. Commun.* 4456

[15] Eichhorn J, Nieckarz D, Ochs O, Samanta D, Schmittel M, Szabelski P J and Lackinger M 2014 On-surface Ullmann coupling: the influence of kinetic reaction parameters on the morphology and quality of covalent networks *ACS Nano* **8** 7880

[16] Cai J M *et al* 2010 Atomically precise bottom-up fabrication of graphene nanoribbons *Nature* **466** 470

[17] Treier M, Pignedoli C A, Laino T, Rieger R, Müllen K, Passerone D and Fasel R 2011 Surface-assisted cyclodehydrogenation provides a synthetic route towards easily processable and chemically tailored nanographenes *Nat. Chem.* **3** 61

[18] Klappenberger F, Zhang Y-Q, Bjork J, Klyatskaya S, Ruben M and Barth J V 2015 On-surface synthesis of carbon-based scaffolds and nanomaterials using terminal alkynes *Acc. Chem. Res.* **48**

[19] Gao H-Y Y, Franke J-H H, Wagner H, Zhong D, Held P-A A, Studer A and Fuchs H 2013 Effect of metal surfaces in on-surface Glaser coupling *J. Phys. Chem.* C **117** 18595

[20] Gao H-Y Y, Wagner H, Zhong D, Franke J-H, Studer A and Fuchs H 2013 Glaser coupling at metal surfaces *Angew. Chem., Int. Ed.* **52** 4024

[21] Gao H-Y Y, Zhong D, Mönig H, Wagner H, Held P-A, Timmer A, Studer A and Fuchs H 2014 Photochemical Glaser coupling at metal surfaces *J. Phys. Chem.* C **118** 6272

[22] Colazzo L, Sedona F, Moretto A, Casarin M and Sambi M 2016 Metal-free on-surface photochemical homocoupling of terminal alkynes *J. Am. Chem. Soc.* **138** 10151

[23] Zwaneveld N A A, Pawlak R, Abel M, Catalin D, Gigmes D, Bertin D and Porte L 2008 Organized formation of 2D extended covalent organic frameworks at surfaces *J. Am. Chem. Soc.* **130** 6678

[24] Ourdjini O *et al* 2011 Substrate-mediated ordering and defect analysis of a surface covalent organic framework *Phys. Rev.* B **84** 125421

[25] Faury T, Clair S, Abel M, Dumur F, Gigmes D and Porte L 2012 Sequential linking to control growth of a surface covalent organic framework *J. Phys. Chem.* C **116** 4819

[26] Weigelt S *et al* 2007 Covalent interlinking of an aldehyde and an amine on a Au(1 1 1) surface in ultrahigh vacuum *Angew. Chem., Int. Ed.* **46** 9227

[27] Treier M, Richardson N V and Fasel R 2008 Fabrication of surface-supported low-dimensional polyimide networks *J. Am. Chem. Soc.* **130** 14054

[28] Schmitz C H, Ikonomov J and Sokolowski M 2009 Two-dimensional ordering of poly(p-phenylene-terephthalamide) on the Ag(1 1 1) surface investigated by scanning tunneling microscopy *J. Phys. Chem.* C **113** 11984

[29] Díaz Arado O, Mönig H, Wagner H, Franke J-H H, Langewisch G, Held P A, Studer A and Fuchs H 2013 On-surface azide-alkyne cycloaddition on Au(1 1 1) *ACS Nano* **7** 8509

[30] Bebensee F, Bombis C, Vadapoo S-R, Cramer J R, Besenbacher F, Gothelf K V and Linderoth T R 2013 On-surface azide-alkyne cycloaddition on Cu(1 1 1): does it 'click' in ultrahigh vacuum? *J. Am. Chem. Soc.* **135** 2136

[31] Krüger J *et al* 2016 Tetracene formation by on-surface reduction *ACS Nano* **10** 4538

[32] Krüger J *et al* 2017 Decacene: on-surface generation *Angew. Chem., Int. Ed.* **56** 11945

[33] Olszowski P, Zapotoczny B, Prauzner-Bechcicki J S, Vilas-Varela M, Pérez D, Guitián E, Peña D and Szymonski M 2015 Aryl halide C–C coupling on Ge(0 0 1):H surfaces *J. Phys. Chem.* C **119** 27478

[34] Marina V M, Yuji O, Elisseos V, Kenji W, Takashi T, Christian J and Masakazu A 2016 Self-assembled diacetylene molecular wire polymerization on an insulating hexagonal boron nitride (0 0 0 1) surface *Nanotechnology* **27** 395303

[35] Abel M, Clair S, Ourdjini O, Mossoyan M and Porte L 2011 Single layer of polymeric Fe-phthalocyanine: an organometallic sheet on metal and thin insulating film *J. Am. Chem. Soc.* **133** 1203

[36] Bombis C, Kalashnyk N, Xu W, Lægsgaard E, Besenbacher F and Linderoth T R 2009 Hydrogen-bonded molecular networks of melamine and cyanuric acid on thin films of NaCl on Au(1 1 1) *Small* **5** 2177

[37] Bombis C, Ample F, Lafferentz L, Yu H, Hecht S, Joachim C and Grill L 2009 Single molecular wires connecting metallic and insulating surface areas *Angew. Chem., Int. Ed.* **48** 9966

[38] Pavlicek N, Schuler B, Collazos S, Moll N, Perez D, Guitian E, Meyer G, Pena D and Gross L 2015 On-surface generation and imaging of arynes by atomic force microscopy *Nat. Chem.* **7** 623

[39] Pavlicek N and Gross L 2017 Generation, manipulation and characterization of molecules by atomic force microscopy *Nat. Rev. Chem.* **1** 0005

[40] Rahe P, Kittelmann M, Neff J L, Nimmrich M, Reichling M, Maass P and Kühnle A 2013 Tuning molecular self-assembly on bulk insulator surfaces by anchoring of the organic building blocks *Adv. Mater.* **25** 3948

[41] Rahe P, Lindner R, Kittelmann M, Nimmrich M and Kühnle A 2012 From dewetting to wetting molecular layers: $C_{60}$ on $CaCO_3$(1014) as a case study *Phys. Chem. Chem. Phys.* **14** 6544

[42] Baer D R and Blanchard D L 1993 Studies of the calcite cleavage surface for comparison with calculation *Appl. Surf. Sci.* **72** 295

[43] Kittelmann M, Rahe P, Nimmrich M, Hauke C M, Gourdon A and Kühnle A 2011 On-surface covalent linking of organic building blocks on a bulk insulator *ACS Nano* **5** 8420

[44] Guo C, Wang Y, Kittelmann M, Kantorovitch L, Kühnle A and Floris A 2017 Mechanisms of covalent assembly on a bulk insulating surface *J. Phys. Chem.* C **121** 10053

[45] Kittelmann M, Nimmrich M, Lindner R, Gourdon A and Kühnle A 2013 Sequential and site-specific on-surface synthesis on a bulk insulator *ACS Nano* **7** 5614

[46] Lindner R, Rahe P, Kittelmann M, Gourdon A, Bechstein R and Kühnle A 2014 Substrate templating guides the photoinduced reaction of $C_{60}$ on calcite *Angew. Chem., Int. Ed.* **53** 7952

[47] Richter A, Haapasilta V, Venturini C, Bechstein R, Gourdon A, Foster A S and Kühnle A 2017 Diacetylene polymerization on a bulk insulator surface *Phys. Chem. Chem. Phys.* **19** 15172

[48] Söngen H, Bechstein R and Kühnle A 2017 Quantitative atomic force microscopy *J. Phys.: Condens. Matter* **29** 274001

[49] Paris C, Floris A, Aeschlimann S, Neff J, Kling F, Kühnle A and Kantorovich L 2018 Kinetic control of molecular assembly on surfaces unpublished

[50] Schüller L, Haapasilta V, Kuhn S, Pinto H, Bechstein R, Foster A S and Kühnle A 2016 Deposition order controls the first stages of a metal–organic coordination network on an insulator surface *J. Phys. Chem.* C **120** 14730

[51] Paris C, Floris A, Aeschlimann S, Kittelmann M, Kling F, Bechstein R, Kantorovich L and Kühnle A 2016 Increasing the templating effect on a bulk insulator surface: from a kinetically trapped to a thermodynamically more stable structure *J. Phys. Chem.* C **120** 17546

[52] Hohenberg P and Kohn W 1964 Inhomogeneous electron gas *Phys. Rev.* **136** B864

[53] Kohn W and Sham L J 1965 Self-consistent equations including exchange and correlation effects *Phys. Rev.* **140** A1133

[54] Dreizler R and Gross E 1990 *Density Functional Theory* (Berlin: Springer)

[55] Parr R G and Yang W 1989 *Density-Functional Theory of Atoms and Molecules* (New York: Oxford University Press)

[56] Jónsson H, Mills G and Jacobsen K W 1998 Nudged elastic band method for finding minimum energy paths of transitions *Classical and Quantum Dynamics in Condensed Phase Simulations* (Singapore: World Scientific)

[57] Henkelman G and Jónsson H 2000 A climbing image nudged elastic band method for finding saddle points and minimum energy paths *J. Chem. Phys.* **113** 9901

[58] CP2K www.cp2k.org/

[59] Giannozzi P *et al* 2017 Advanced capabilities for materials modelling with QUANTUM ESPRESSO *J. Phys.: Condens. Matter* **29** 30

[60] Kresse G and Furthmüller J 1996 Efficient iterative schemes for *ab initio* total-energy calculations using a plane-wave basis set *Phys. Rev.* B **54** 11169

[61] Goedecker S, Teter M and Hutter J 1996 Separable dual-space Gaussian pseudopotentials *Phys. Rev.* B **54** 1703

[62] Vanderbilt D 1990 Soft self-consistent pseudopotentials in a generalized eigenvalue formalism *Phys. Rev.* B **41** 7892

[63] Blöchl P E 1994 Projector augmented-wave method *Phys. Rev.* B **50** 17953

[64] Perdew J P, Burke K and Ernzerhof M 1996 Generalized gradient approximation made simple *Phys. Rev. Lett.* **77** 3865

[65] Grimme S 2006 Semiempirical GGA-type density functional constructed with a long-range dispersion correction *J. Comput. Chem.* **27** 1787

[66] Grimme S, Antony J, Ehrlich S and Krieg H 2010 A consistent and accurate *ab initio* parametrization of density functional dispersion correction (DFT-D) for the 94 elements H–Pu *J. Chem. Phys.* **132** 15410

[67] Kristensen R, Stipp S L S and Refson K 2004 Modeling steps and kinks on the surface of calcite *J. Chem. Phys.* **121** 8511

[68] Ataman E, Andersson M P, Ceccato M, Bovet N and Stipp S L S 2016 Functional group adsorption on calcite: I. Oxygen containing and nonpolar organic molecules *J. Phys. Chem.* C **120** 16586

[69] Kittelmann M, Rahe P and Kühnle A 2012 Molecular self-assembly on an insulating surface: interplay between substrate templating and intermolecular interactions *J. Phys.: Condens. Matter* **24** 354007

[70] Maglic J, Lautner D, Bechstein R and Kühnle A 2017 Desorption of benzene, pyridine and aniline from calcite (10.4) unpublished

[71] Ataman E, Andersson M P, Ceccato M, Bovet N and Stipp S L S 2016 Functional group adsorption on calcite: II. Nitrogen and sulfur containing organic molecules *J. Phys. Chem.* C **120** 16597

[72] Gutzler R *et al* 2014 Ullmann-type coupling of brominated tetrathienoanthracene on copper and silver *Nanoscale* **6** 2660

[73] Kittelmann M, Nimmrich M, Neff J L, Rahe P, Gren W, Bouju X, Gourdon A and Kühnle A 2013 Controlled activation of substrate templating in molecular self-assembly by deprotonation *J. Phys. Chem.* C **117** 23868

[74] Núñez-Regueiro M, Marques L, Hodeau J L, Béthoux O and Perroux M 1995 Polymerized fullerite structures *Phys. Rev. Lett.* **74** 278

[75] Park S, Han H, Kaiser R, Werninghaus T, Schneider A, Drews D and Zahn D R T 1998 The phototransformation of C60 thin films on GaAs(1 0 0) studied by *in situ* Raman spectroscopy *J. Appl. Phys.* **84** 1340

[76] Onoe J, Nakayama T, Nakao A, Hashi Y, Esfarjani K, Kawazoe Y, Aono M and Takeuchi K 2000 *In situ* FTIR, XPS, and STM studies of the nano-structure of a photopolymerized $C_{60}$ film *Mol. Cryst. Liq. Cryst.* **340** 689

[77] Nakaya M, Nakayama T and Aono M 2004 Fabrication and electron-beam-induced polymerization of C nanoribbon *Thin Solid Films* **464–5** 327

[78] Okawa Y, Akai-Kasaya M, Kuwahara Y, Mandal S K and Aono M 2012 Controlled chain polymerisation and chemical soldering for single-molecule electronics *Nanoscale* **4** 3013

[79] Nakaya M, Okawa Y, Joachim C, Aono M and Nakayama T 2014 Nanojunction between fullerene and one-dimensional conductive polymer on solid surfaces *ACS Nano* **8** 12259

[80] Fahsi K, Deschamps J, Chougrani K, Viau L, Boury B, Vioux A, van der Lee A and Dutremez S G 2013 Stability and solid-state polymerization reactivity of imidazolyl- and benzimidazolyl-substituted diacetylenes: pivotal role of lattice water *CrystEngComm* **15** 4261

[81] Glaser C 1869 Beiträge zur Kenntniss des Acetenylbenzols *Ber. Dtsch. Chem. Ges.* **2** 422

[82] Björk J, Zhang Y-Q, Klappenberger F, Barth J V and Stafström S 2014 Unraveling the mechanism of the covalent coupling between terminal alkynes on a noble metal *J. Phys. Chem.* C **118** 3181

[83] Eichhorn J, Heckl W M and Lackinger M 2013 On-surface polymerization of 1,4-diethynylbenzene on Cu(1 1 1) *Chem. Commun.* **49** 2900

[84] Richter A, Vilas-Varela M, Peña D, Bechstein R and Kühnle A 2017 Homocoupling of terminal alkynes on calcite (10.4) *Surf. Sci.* accepted (https://doi.org/10.1016/j.susc.2017.12.012)